International Journal of Modern Physics D
(2020) 2050050 (27 pages)

DOI: 10.1142/S0218271820500509

Measurement of geophysical effects on the large-scale gravitational-wave interferometer

A. V. Gusev*,‡, E. Majorana†,§, V. N. Rudenko*,¶, and V. D. Yushkin*,‖

*Sternberg Astronomical Institute,
Lomonosov Moscow State University,
Universitetsky pr. 13, Moscow 119234, Russia

†Univ. Roma "Sapienza" and INFN Roma,
p. Aldo Moro 10, Roma, Italy

‡avg@sai.msu.ru
§ettore.majorana@roma1.infn.it
¶valentin.rudenko@gmail.com
‖yusvic@yandex.ru

Received 4 June 2019
Revised 6 March 2020
Accepted 21 March 2020
Published 26 May 2020

Geophysical application of large free-mass laser interferometers, which had been designed merely for the detection of gravitational radiation of an astrophysical nature, are considered. Despite the suspended mass-mirrors, these interferometers can be considered as two coordinate meters even at very low frequency ($f < 10^{-3}$ Hz) are rather accurate two-coordinate distance meters. In this case, the measurement of geodynamic deformations looks like a parallel product of long-term observations dictated by the task of the blind search for gravitational waves (GW) of extraterrestrial origin. Compared to conventional laser strain meters, gravitational interferometers have the advantage of an increased absolute value of the deformation signal due to the 3–4 km baseline. The magnitude of the tidal variations of the baseline is 150–200 microns, leading to conceive the observation of the fine structure of geodynamic disturbances. This paper presents the results of processing geophysical measurements made on a Virgo interferometer during test (technical) series of observations in 2007–2009.

The specific design of mass-mirrors suspensions in the Virgo gravitational interferometer also creates a unique possibility of separating gravitational and deformation perturbations through a recording mutual angular deviations of the suspensions of its central and end mirrors. It gives a measurement of the spatial derivative of the gravity acceleration along with the geoid of the Earth. In this mode, the physics of the

interferometer is considered with estimates of the achievable sensitivity in the application to the classical problem of registration of oscillations of the inner Earth's core.

Keywords: Gravitational wave interferometer; laser interferometer with suspended mirrors; geodynamic effects measurement.

1. Introduction

Large-scale laser interferometers with suspended mirrors were designed for the observation of gravitational waves from astrophysical objects. Just as they were constructed, the hypothesis of exploiting them for geophysical applications was promptly proposed and developed, Refs. 1–8. In this paper we report about the first experimental studies aimed to global geodynamic measurements, by means of Virgo.

At the very low-frequency range $(10^{-4} - 10^{-6})$ Hz, this setup can be considered as a "deformation-gravitational" measuring apparatus, as it also provides information on the ground variations of geophysical fields. The longitudinal deformations on the N–S and W–E components are tracked by the driving voltage of the length correction of the 3-km-long resonant cavities along the arms of the Michelson interferometer. Local tilt deformations (variations of the local normal vector) can be extracted from correcting signals of angular positions of each mirror using the optical laser beam feeding the interferometer. Moreover, changes of the differential angle of the suspended mirrors, so-called mutual angle of plummets (or plumb lines), induced by variations of the land gravitational gradient, can be measured as correction signals of collinearity of the beam with the optical axes of interferometer arms (FP-resonators). Remarkably, KAGRA, a new underground 3-km-long detector with seismic isolation concept inspired to Virgo has been set in operation in Japan. A 1.5-km-long laser strain meter was also installed along one of its arms to monitor the stability of tunnel rocks.[10]

The experimental data on the noise level in the circuits of control systems were investigated in the frequency band of the detection of GW. In low frequency range (< 0.1 Hz), which is interesting for geophysics, the noise data have not been analysed in detail. The lowest frequency band $\sim$1 Hz, studied experimentally, has the spectral amplitude of mirrors angular fluctuations $\sim(10^{-7} - 10^{-8})\,\mathrm{rad/Hz^{-1/2}}$. The possibility of extrapolating this estimate to the lower frequency range around $\sim 10^{-4}$ Hz is not clear *a priori* and requires additional measurements. However, such measurements are only feasible during the sufficiently long observation series (about a month or more).

The first long-term scientific run of astrophysical observations (first scientific run, VSR-1) was performed in 2007. SAI MSU group, through a formal agreement with Virgo, undertook the analysis of data of low frequency channels with the goal to experimentally study the quasi-static noise and search for possible geophysical effects. The overall period studied was 4.5-month-long series of quasi-continuous observations, from 18.05.07 to 10.10.07. Even if relatively stable, time series were

affected by a relatively large number of interruptions due to operation set-point unlocks, affecting the quality of the affordable geodynamical reconstruction. After VSR-1, suspension control data, undersampled at 1 Hz, and covering about 75% of the neat operation time, were studied at SAI MSU and the first analysis was carried out. The results of the analysis of this data set and those carried out later (VSR-2) are presented.

2. Schematic layout of Virgo interferometer

The principle of operation of the Virgo interferometer as a detector of GW is based on the fact that the GW carries the oscillating gravitational gradient and changes the differential length of the interferometer arms. The mirrors can be considered as free bodies at frequencies much larger than their suspension resonances. The overall apparatus is composed of several optical resonators, combining Fabry-Pérot (FP) and Michelson interference to detect differential arm-length variation, see Fig. 1(a).

The FP cavities provide optical enhancement of the Michelson arms, thanks to Finesse parameter, increasing GW-optical conversion gain. The total number of photon round-trips in the first version of the Virgo was roughly 50, which, with a physical base of 3 km, gives an equivalent arm length of 150 km. (Recently, the optical configuration has been significantly changed, and the equivalent length is 1200 km). Although the test masses of the detector are mechanically and acoustically isolated, the overall apparatus is still subject to various sources of noise caused by external disturbances, such as seismic activity, wind stress on buildings, ground shaking caused by human activity, as well as by other natural geophysical perturbations.

To keep the detector in operation, passive seismic filters, constituted by cascaded of pendulum and springs under inertial damping of internal modes, and active position control upon interference signal, are used, Fig. 1(b). The last stage of test mass suspension (marionette), meant to orientate it, also plays a role in the overall passive attenuation of the chain that reaches respectively 240 dB for vertical and 280 dB for horizontal directions at 10 Hz.[11] Positional and angular control of the suspended elements of the Virgo interferometer is based on the modulation technique (this is the so-called Pound–Drever–Hall technique.[12]) Correction signals are derived by the degrees of freedom of the main optical beam of the interferometer (global control, GC). Auxiliary position control beams, forming optical levers, are also used, in local control scheme (LC), to acquire the lock, that sets the distance between all the optical elements forming the Fabry-Perot cavities. Schematically, the combination of angular and longitudinal control sensing of the suspended mirrors of a cavity is sketched in Fig. 1(b).

Single-point mechanical suspension scheme is adopted downwards through the whole 9.07 m-long cascade of 7 pendulum stages of SA. Single-point suspension turns to be a unique characteristic to perform angular differential measurements. Below the last single-point suspended stage (marionette) two looped steel wires

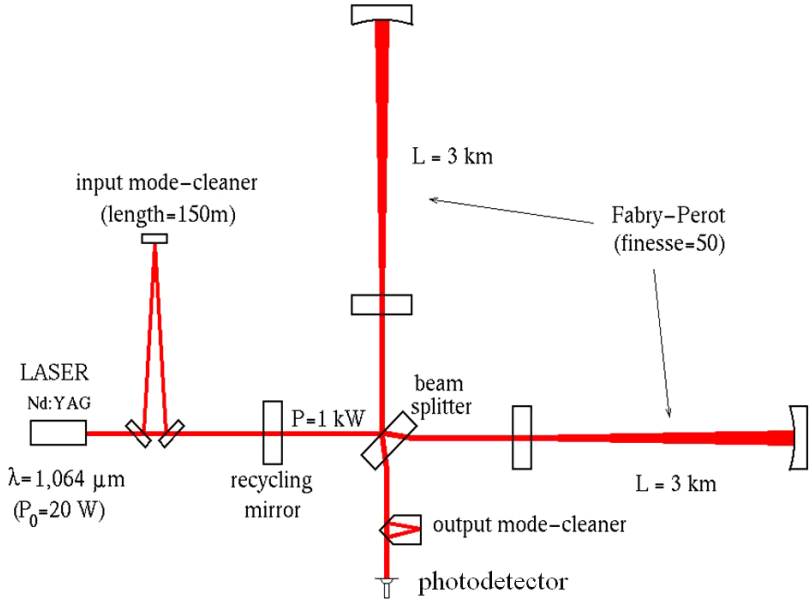

(a)

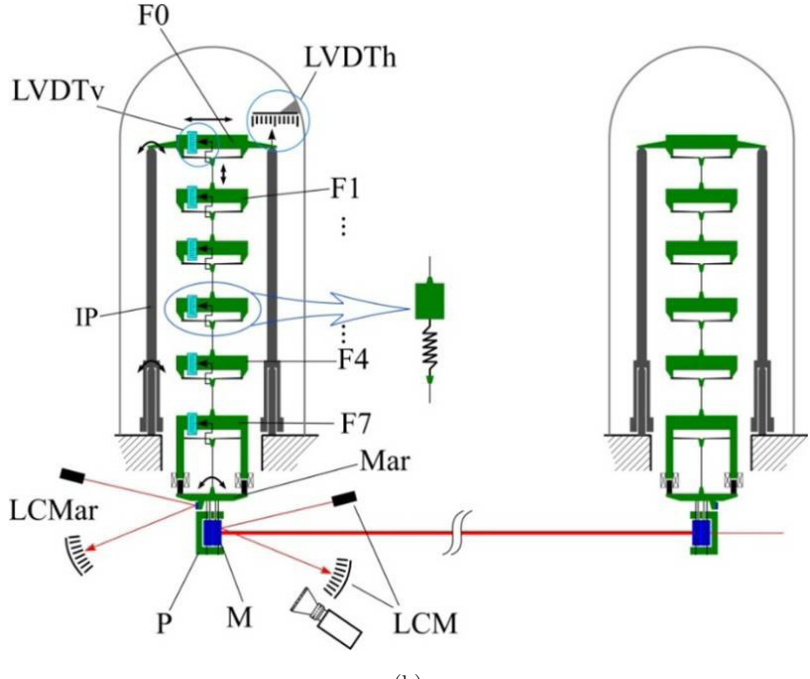

(b)

Fig. 1. (a) Principal configuration of the Virgo interferometer (from LV documents); (b) Arm's mirrors suspension on SA with global and local position control.

are used to orientate the mirrors (now four fused silica fibers). A more detailed presentation of the principles and techniques of SA operation as part of the GC and LC circuits, see in Refs. 11 and 13.

When the feedback circuits of the interferometer are locked, they provide a measuring of quadrupole deformation of the setup. It includes the residual internal instrumental noise and external disturbances. The local control system sensors work almost entirely in monitoring mode. It should be noticed that the mirrors of the interferometer, with respect to measurement of the geodynamical effects, are equivalent to the probe masses directly fixed on some equivalent ground platform obtained by subtracting all local disturbances at the land. Hence, GW interferometers at quasistatic frequencies can be considered as a complex geophysical instrument composed of two-coordinate horizontal deformometer (strain meter) and two 3 km-separated pairs of tiltmeters. The arms of the deformometer and the tilt-angle pairs are oriented (approximately) in the directions N-S and E-W. Tidal changes in arm length L in the N-S and E-W directions reach 150 and 250 microns (or 50 and 83 nano strain), respectively. Remarkable that signals of geophysical perturbation dominate in comparison to the internal (instrumental) noises of VIRGO due to the large-scale of the setup. During the operation, the accuracy of the confinement of the longitudinal size of the FP resonators in the arms of the interferometer is 10^{-12} m RMS, and accuracy of retention of the mutual angular orientation of mirrors 10^{-9} rad RMS.[11,13,14]

3. Measurement of Tidal Deformations with VIRGO

Presenting the data of observations VSR-1 and VSR-2,[11,13] we would like to note that the non-conventional analysis, leading to reconstruct geodynamical effects through mirror suspension control system of a large-scale GW detector was original. The absolute value of tidal signal recorded by this setup turns out to be (30–100) times larger then the one for typical instruments with the base of (10–100) m. In principle, it should facilitate the observation of weak geodynamic effects. So as it provides the gain against the background of instrumental (internal) noise of the interferometer. However, the technical possibility of this advantage is determined by the achievable value of the signal-to-noise ratio.

Below there are results of the analysis of two relatively long observation series of Virgo: VSR-1, containing 4.5 months (135 days), quasicontinuous observations (from 18.05.2007 to 10.10.2007), and VSR-2 containing almost 5.5 months or 162 days (from 07.06.2009 to 16.11.2009). Tidal perturbation was also observed on the LIGO interferometers but according to a different principle, through the amplitude modulation of the harmonic on free spectral range frequency. The effect appears at the main interferometer's output due to the noise luminosity of the FP mode neighbor to the central one at the pump frequency,[15–17] see also Ref. 18. The main goal of Refs. 15 and 16 was to investigate the possibility of laser GW detectors

working in the lower frequency range due to the suppression (compensation) of tidal deformations.

3.1. *Registering of longitudinal displacements*

Data of horizontal deformations are taken from the feedback circuit controlling of the inverted pendulum (IP) at Fig. 1(b). The primary source is the driver of the LVDT (Linear Variable Displacement Transducer) located on the top platform (filter F0) of the SA. Its reference is fixed on the ground, and it senses the drag actuated between the ground and the IP top meant to maintain the optical length at the level of the test mass. With a new lock, the distance between the mirrors (3 km) is restored with an error of not more than 30 μm, if the interval between the grips was not too long (less than 1.5 h).

Experimental records of the horizontal deformation of the northern arm are shown at Fig. 2(a) (the blue curve): (10 days VSR-1)[11] and in Fig. 2(b) (5 days VSR-2).[13] This is raw data without any fitting procedure. The expected tidal deformation (theoretical) is shown in the same figures (the green curve). Theoretical deformation was calculated using a special program ETGTAB, developed by Wenzel,[19] with the substitution of tidal gravitational potential taken from the well-known program developed by Tamura.[20] This approximation takes into account ∼1200 tidal waves calculated for a rigid Earth model, with an amplitude factor of 1.0 and a phase delay less the 0.03 arc degree. However, for waves with a longer period, the amplitude factor 1.16 was chosen, and for the phase delay, 0.01 arc degree ($1.74 \cdot 10^{-4}$ rad). For the Virgo interferometer, the local coordinates and corresponding directions of the arms are known. Fragments of data records with acceptable quality were selected for detailed geophysical analysis (without breaks, peaks, sharp vertical jumps). The results are given in Fig. 2. The deviation of δ between the amplitudes of the theoretical and experimental curves was estimated using the least mean squares (LMS) method.[21] For the first observational series VSR1, the average deviation was $\delta = 1.030 \pm 0.03$, for the second — VSR2, $\delta = 1.005 \pm 0.003$, i.e. the overall quality of the records in the second series was improved. Estimates of phase delays for the same selected pieces of records resulted in $\Delta\theta = (2.4 \pm 0.4)$ arc degree, $(4.18 \pm 0.68) \cdot 10^{-2}$ rad for both the VSR-1 and VSR-2 series. However, this value is not indicated because of the large size of the confidence interval. Actually, this corresponds to a delay of about 10 minutes between the theoretical forecast and the observed deformation.

For spectral analysis, we used a total observation time of 135 days in VSR-1[11,22] and 162 days in VSR-2.[13] The results of the spectral analysis of the horizontal deformations of the arms are presented: for the northern arm in Figs. 3(a) and 3(c) and for the western arm in Fig. 3(b) and 3(d) (all figures have the same scale according to time series duration). The spectra look very similar and coincide with the theoretical spectra calculated for given local coordinates and the corresponding arm directions, – N:19°25'57".9650 and W: 289°25'59".10.[23]

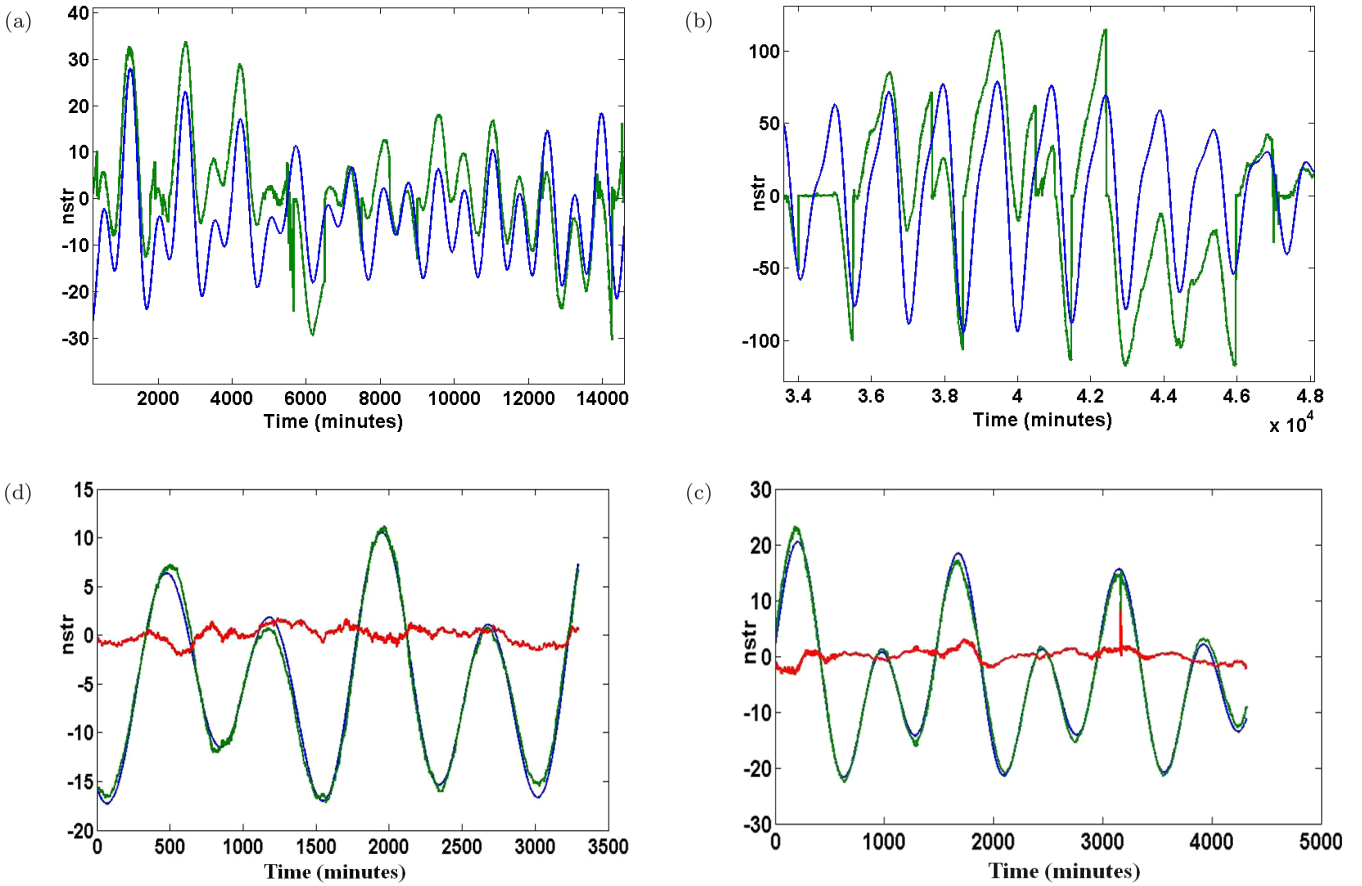

Fig. 2. The north arm tidal deformation (a) VSR-1 , (b) VSR-2 (blue — theory, green — experiment). Comparison after fitting (c) VSR-1 , (d) VSR-2 (green — experiment, blue — theory, red — residuals).

A slight difference in comparing the spectra of VSR-1 and VSR-2 appears partly due to different lengths of processed time series and better data quality during VSR-2. In particular, the daily harmonics during VSR-2 are closer to theoretical calculations (the difference in peak amplitudes is ∼20%, while for VSR-1, this difference was ∼50%. (Notes to spectra images in Fig. 3: visible peaks: semi-diurnal S2: 720 min; y-axis nstr^2/Hz; Sun diurnal S1+P1+K1, 1436-1444 min; Moon diurnal O1:1549 min, Moon semi-diurnal M2 + N2 : 745.749 min).

Figure 3 shows the data of the main groups of tidal waves, according to the classification of Melchior,[24] with their periods. It should be noted that the overall quality of data on tidal deformations of the western arm is worse for the northern one. At the same time, in the east–west direction, the amplitudes of all tidal harmonics are almost twice the amplitudes of the north–south direction. Comparison of the VSR-1 and VSR-2 series shows that after updating the Virgo setup performed between the series, the data quality has improved. A longer continuous recording is required to register a wider range of tides, with more than 20 harmonics; its duration must be at least one year. In that case, the goal of detecting harmonics generated by the movement of the internal Earth's core would be more realistic.

3.2. *Numerical estimates of registered tidal harmonics*

Using the data recorded during of the VSR-2 observational run (162 days), we estimated parameters of the registered groups of tidal waves using the maximum likelihood method (4 waves for the N-arm and 5 for the W-arm). Their periods and amplitudes are presented in Table 1, columns 6, 7, and 9, 10. We also calculated the theoretically expected tidal signals at the intervals of the same duration. The theoretical wave amplitudes are presented in columns 5, 8. The first four columns of the table contain code numbers, names and periods of the main waves, taken from the book.[24] One can conclude a satisfactory coincidence of the classical tidal theory and experiment.

3.3. *Search for anomalous resonances*

Data records with a continuous duration of more than 12 hours were selected. For each segment, the mean (tidal) evolution and discrepancy (variance) were determined by the LMS method.[21] A total of 72 data chunks were found for each interferometer arm. The temporal evolution of the residuals (deviation) of amplitudes for both arms is shown in at Fig. 4(a) (N-arm — blue, W-arm — red). The mean values (the so-called "average ratio") in Fig. 4(a) are marked with dotted lines. It confirms that W-arm is noisier than N-arm. The spectral composition of the residuals is shown in Fig. 4(b).

Interest in this spectrum is associated with the search for nonclassical effects in tidal deformations. Modern approaches to theoretical models of tides consider various subtle effects.[25] The dynamics of the Sun-Earth-Moon system are calculated, taking into account the evolution of the mass center of the Earth-Moon as it

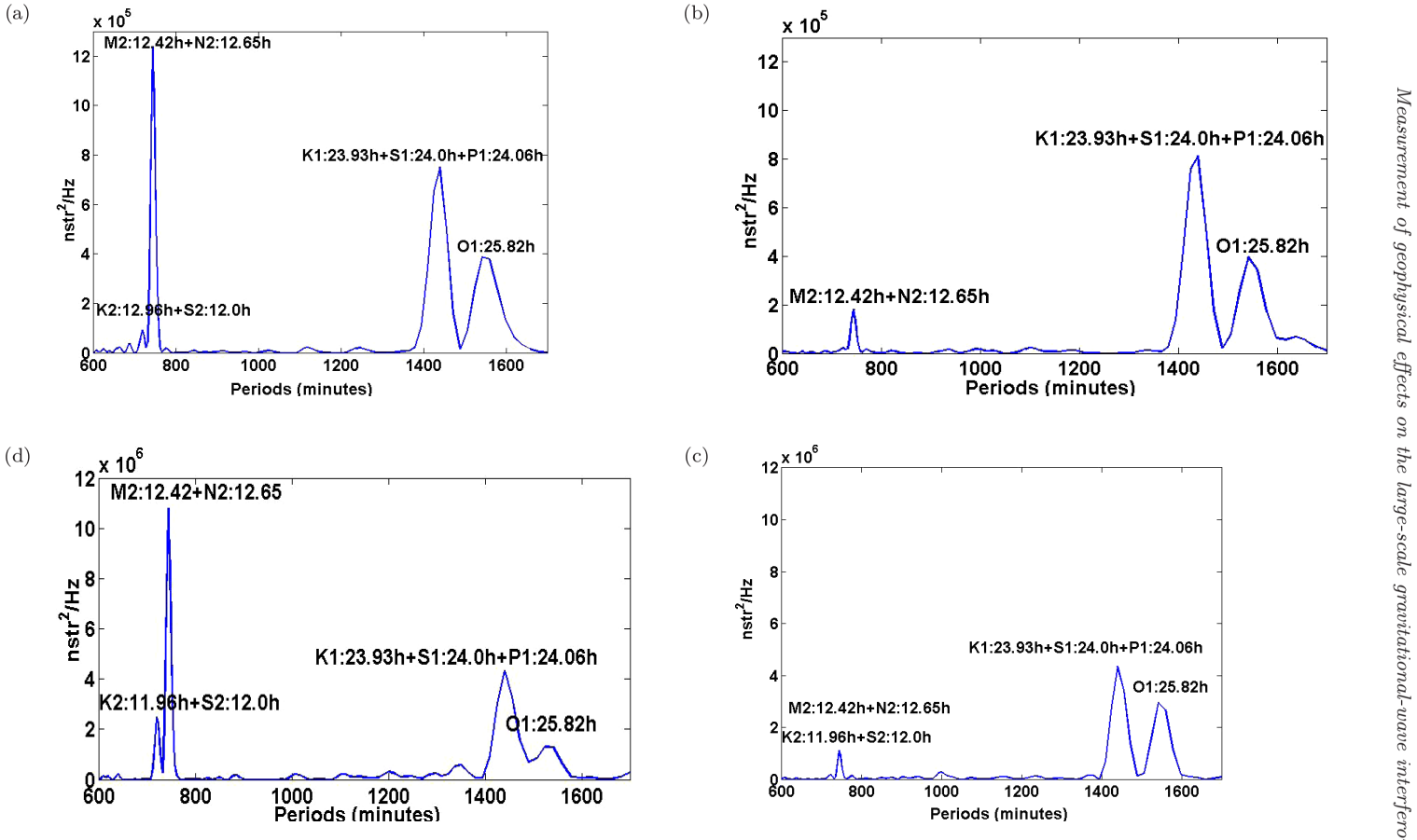

Fig. 3. Spectra of tidal deformation: north arm (a) VSR-1, (d) VSR-2; west arm (b) VSR-1, (c) VSR-2.

Table 1. Estimates of nominal of tidal harmonics from the VSR-2 data.

Waves			Theor. period, hours	Nothern arm			Western arm		
				Theor. amplitude, μm	VIRGO (162 days)		Theor. amplitude, μm	VIRGO (162 days)	
Groups		Name			Period, hours	Amplitude, μm		Period, hours	Amplitude, μm
from	to								
1	2	3	4	5	6	7	8	9	10
Semidiurnal									
1009	1021	K2	11.96	16	11.993	13	6	11.998	5
981	947	M2	12.42	33	12.421	30	13	12.422	11
Diurnal									
559	592	K1	23.93	20	23.907	15	30	23.902	14
538	554	P1	24.06	5	—	—	7	24.095	9
429	488	O1	25.82	15	25.831	14	22	25.794	17

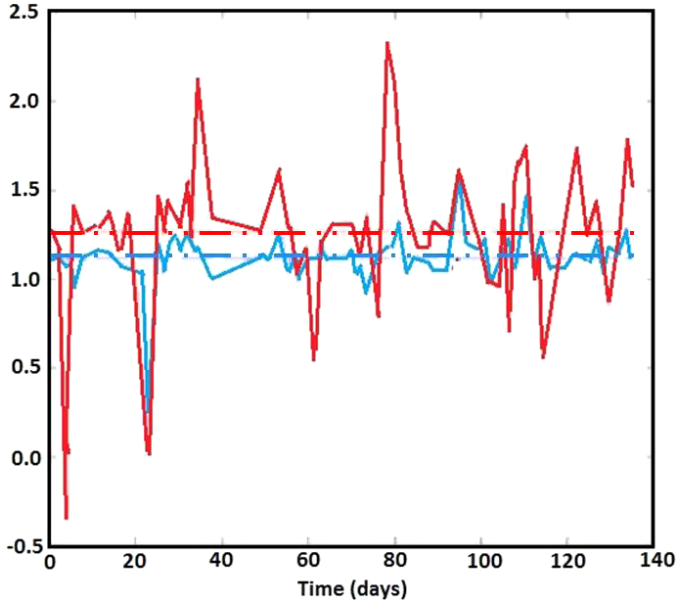

(a)

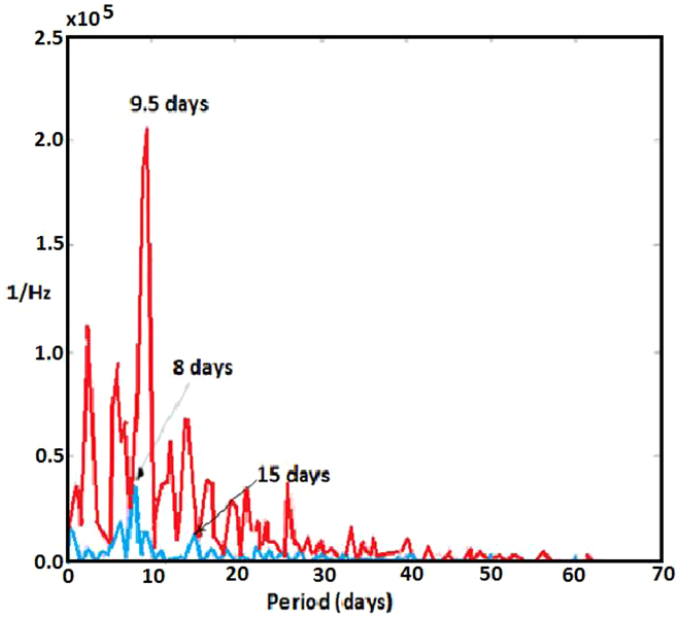

(b)

Fig. 4. (a) Residuals of tidal deformations for north (blue) and west (red) arm; (b) Spectra of residuals.

moves along the solar orbit. In the orbital process, the position of this mass center located inside the Earth is shifted relative to the center of the Earth. This leads to the appearance of additional weak harmonic perturbations in the classical tidal spectrum of the Earth.

In Ref. 26 the occurrence of relatively short harmonics with a period of about two weeks, three months, and longer is predicted.

The physics of this phenomenon is associated with the expected movement of the inner Earth's core relative to the center of mass of the Earth-Moon. The spectrum is shown in Fig. 4(b) contains components with periods of ∼9.5 and ∼15 days, which, in principle, can be considered as experimental candidates to confirm the theory.[25,26] However, the presence of significant noise content in Fig. 4(b) makes the reliability of these peaks not too high — it barely reaches 30% with the level of confidence of 0.95. Thus, these estimates and the associated peaks in Fig. 4(b) should be confirmed by more accurate measurements.

3.4. *Tidal tilt detection*

The overlap of local drifts of various nature and tidal drifts is globally compensated by the automatic control system based on position and wave-front sensing the main beam to keep the FP cavities aligned and beam centered on mirrors. Then the extraction of tidal tilt signature in VSR-1 and VSR-2 data was non-trivial. The only way is to combine local control signals with global control ones. A further study of geodynamical effects using new data has to take the combination in suitable account.

4. Virgo as an Angular Gravity Gradiometer

In Refs. 2 and 3, the GW interferometer on suspended mirrors was considered for the measurement of the mutual deflection of spatially separated plummets ("plumb lines") on the Earth's surface. The reference frame of deviations is the optical beam, see Fig. 5(a). Also, in the case of suspension of the beam source (laser) near the input mirror, such a reference frame (line of the beam) is insensitive to the deformation disturbances of the Earth's surface. Then the variation of the mutual angle of suspension wires depend only on the gravitational perturbations of the plumb lines (gravity vectors). The interferometer turns into an angular gravity gradiometer. In Refs. 2 and 3 it was proposed to use such a tool for detecting vibrations of the inner core of the Earth. However, in the current apparatus, and thanks to the overall control systems, the position of the beam can be considered as injected on a line that is perpendicular to the input mirrors of the cavities and centered on the long FP cavity mirrors.

As a result, the tilt deformation of the Earth's surface is contained in the angular noise of a reference line, i.e. the laser beam. The measurement scheme proposed in Refs. 2 and 3 turns out to be unrealistic.

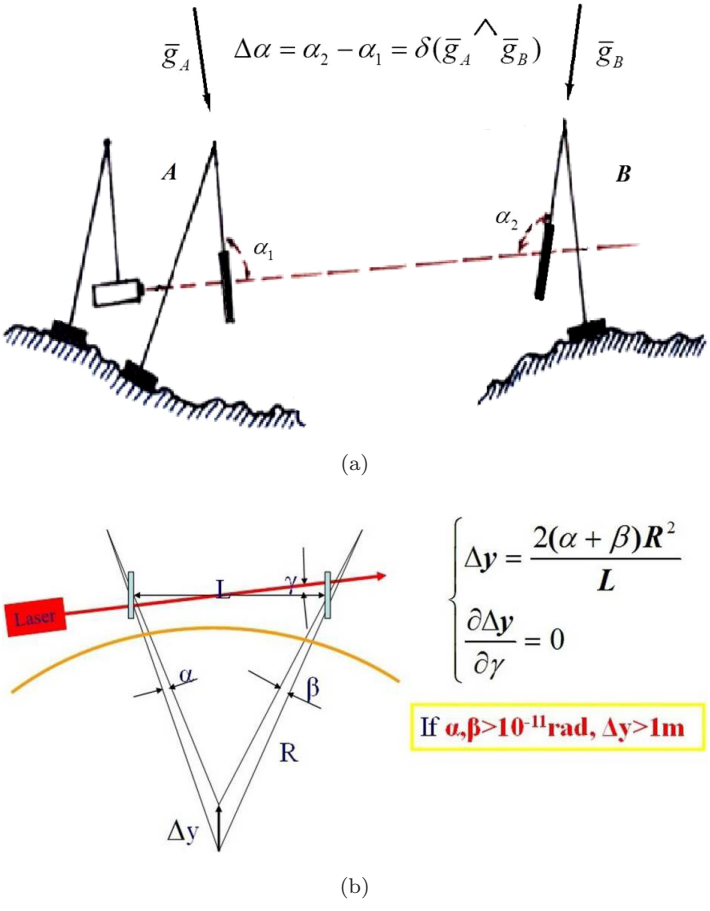

Fig. 5. (a) Principle scheme of the angular gravity gradiometer. (b) Principal scheme of the beam tilts compensation under a measuring of axial core oscillations.

A joint research group Virgo-SAI-MSU studied the possibility of preserving the idea of the Virgo instrument as the "gravitational angular gradiometer". Some specific methods for its practical realization were developed. In this section results of these considerations are presented.

A new approach to angular measurements with Virgo consists in using the old geophysical idea of a "differential tiltmeter" formed by two ordinaries, but spatially distanced instruments.[27] In the case of Virgo, this idea turns out to be very fruitful and comes back to the possibility of a pure "gravity-inertial meter". Below we are discussing it more in detail.

In Ref. 27, two tiltmeters spatially separated on a broad base were considered just for the problem of detecting the Earth's inner core movements. The effect is characterized by the magnitude of the mutual deviation of the gravity vectors. The deformation variations of local normal create a dominant noise background, which

prevents the detection of a weak differential effect. In a search for a solution, the authors of Ref. 27 analyzed the correlation coefficient of different local normals deviations, selecting the optimal ratio between the size of the base and the long deformation waves at the frequencies of inner core oscillations. The deformation noise can be suppressed proportionally to the correlation coefficient, which, however, could not be entirely estimated in the paper.[27]

A radically different situation occurs in the case of a Virgo instrument. The light beam, as the carrier of the "deformation noise", serves as a standard reference line for reading out angles of g vector suspension of the front and end mirrors. It means that the correlation coefficient of their angular deviations is equal to one (on modulo). In principle, selecting the desired algebraic combination of two angles, one can reduce this noise to zero, while filtering the useful differential effect of gravity-inertial perturbations.

The possibility of measuring the mutual deviation of spatially separated suspensions (plumb lines) is provided by the technique of angular control of mirrors in the Virgo interferometer (Sec. 2). A necessary condition for the applicability of this technique for this task: — one wire (simple strand) suspension of mirrors[3,6,8] also in this case plays a crucial role.

Interferometers LIGO and GEO use a double-stranded or looped type of mirror suspension (doll marionette) in which the mirror, obeying the angular variations of the gravity vector, deviates without changing its surface tilt (its surface moves parallel to itself). In VIRGO, a single strand suspension is used over the entire length of the 10-meter-5-link filter in Fig. 1(b). It is just such specificity of the Virgo suspension that makes this instrument uniquely suitable for measuring mutual angular deviations of spatially distanced plumb lines. Underground GW interferometer KAGRA[9] also realized one wire suspension similar to the VIRGO type but besides it has also the 1500-m-long conventional strain-meter in the Kamioka mine installed along one arm of the detector.[10]

4.1. *Variations of the gravity acceleration produced by the inner core movement*

Let us consider a small oscillation of the inner core along with the Earth rotation axis (so-called Slichter mode[28]).

Assuming the displacement amplitude $r = 1\,\mathrm{m}$ at Fig. 5(b). One can easily calculate of variations of the gravity acceleration at the Earth surface $\Delta g = 10^{-7}\,\mathrm{Gal}$ ($100\,\mathrm{nGal}$), as well as the plumb line deflection $\Delta\alpha \approx 10^{-10}\,\mathrm{rad}$ (the differential effect $\sim 10^{-13}\,\mathrm{rad}$).

In the model of periodic movement of the core with a cycle of $\tau \approx 4h \sim 10^4\,\mathrm{s}$; under a measurement time of the order of the oscillation period, the maximum permissible for registration noise spectral densities is $\mathrm{NSD}_g = 20\,\mu\mathrm{Gal/Hz^{1/2}}$, $\mathrm{NSD}_\alpha = 10^{-8}\,\mathrm{rad/Hz^{1/2}}$.

4.2. *Methods for compensating of deformation tilts*

For registering a mirror's angular variations caused by the inner core oscillations two types of special data processing were proposed. The first one (adapted for the Slichter mode detection) consists in the transition to a new observable variable Δy compiled as $\Delta y = 2(\alpha+\beta)R^2/L$,[13] where α, β are the angular deflections of plumb lines, at Fig. 5(b). This variable is independent of the angular perturbations of the beam γ, i.e. $\partial\Delta y/\partial\gamma = 0$ (here R is the Earth's radius and L is the length of the arm). However, it should be noticed that such a scheme is ideal when the interferometer is located in areas close to the Earth's pole, losing efficiency at small latitudes. For the location of the Virgo interferometer, the signal suppression factor is 0.68.

The second method is a more general and does not depend on the specific core oscillations. In principle, it is still based on the correlation of disturbances caused by deflections of the beam for both, front and end, arm mirrors. The principle algorithm of how this scheme works is illustrated in Fig. 6. It depicts one of the interferometer arms with suspended frontal and terminal mirrors. On the suspension, there is also a beam injection bench platform, while the laser is installed on the ground plate. The suspensions are shown schematically: not the entire super-attenuator, but only its principal parts: a single-strand suspension, a marionette, and a two-wire (loop) mirror pickup.

Here, it is appropriate to give information on the principle of a geodetic instrument measuring so-called plumb line deviation. This is just a measurement of the direction of the gravity vector, as a normal to the surface of the geoid, i.e. the surface of equal gravitational potential, defining a "figure of the Earth". For this, a telescope is installed near the plumb line, fixing the direction to a distant stellar object (ideally, a quasar), i.e. setting the direction in the celestial coordinate system. In relation to this direction, the plumb angle is counted. Variations of the normal to the physical platform on which such a device is installed have no effect on its readings. A specific description and characteristics of such a device can be found,

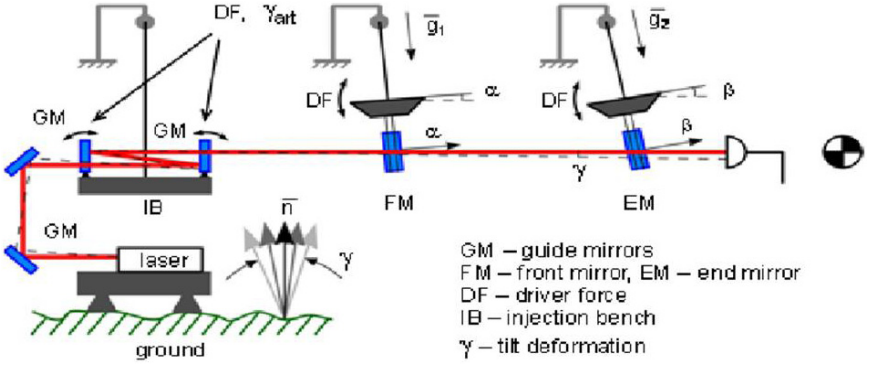

Fig. 6. General scheme of the common beam tilts compensation.

for example, in the links.[29,30] Returning to the idea of the angular gravitational gradiometer Fig 6, we note that here lies the same idea — to get rid of the dominant noise of non-gravitational tilts of the reference line — the optical beam. It is possible when measuring the differential effect of the mutual deviation of spaced plumb lines (in fact, the derivative of the gravity acceleration along its geoid surface). In this case, an appeal to the celestial coordinate system is not required.

In Fig. 6, the ideal instantaneous position of the mirror is shown when the plumb line is deflected. An alignment error signal is transferred to marionette drivers (DF), which provide the position when the surface of the mirror is perpendicular to the laser beam. The amplitude of the driver voltage carries an information about the angle of the deflection of the plumb line. The laser beam radiation through the guide mirrors (GM) is elevated to the interferometer plane and enters the arm cavity at some angle γ to its optical axis. Naturally, changes in this angle are associated with the deformation tilts of the laser.

To explain the deformation compensation method, one uses the list of symbols for the angles and opto-mechanical components in Fig. 6: α — deflection angle of the front mirror, β — deflection angle of the end mirror, γ — deflection angle of the beam, $\theta_1(g_1)$ — deflection angle of the front plummet, $\theta_2(g_2)$ — deflection angle of the end plummet, $\theta_1(g_1) + \theta_2(g_2) = \theta(g_1 + g_2)$ — sum of the deflection angles of two plummets. At last: $\theta(\widehat{g_1\ g_2})$ — the angle of mutual evasion of two plumb lines. The notations of the particular components at Fig. 6 are the following: **GM** — the guiding mirrors, **FM** — the front arm mirror, **EM** — the end arm mirror, **DF** — the correcting force moment, **IB** — the injection beam platform. On this picture all angles are measured in respect of the zero reference level (line) defined by the injection beam platform **IB**.

Equations describing the coupling between these angle variables read as

$$\begin{aligned} \delta\alpha &= \delta\gamma + \delta\gamma_{\text{art}} + \theta_1(g_1), \\ \delta\beta &= \delta\gamma + \delta\gamma_{\text{art}} + \theta_2(g_2). \end{aligned} \tag{1}$$

It can be seen that the angles of the gravity vectors with the reference line are the sum of the angles of the plumb lines and the angles of deviation of the beam (deformation component).

The sum of the variations of these angles practically contains only deformations (considering them dominant in comparison with the variations of the angles of the plumb lines)

$$\delta\alpha + \delta\beta = 2(\delta\gamma + \delta\gamma_{\text{art}}) + \theta(g_1 + g_2) \approx 2(\delta\gamma + \delta\gamma_{\text{art}}). \tag{2}$$

A different of these angle looks like:

$$\delta\alpha - \delta\beta = \theta(\widehat{g_1\ g_2}). \tag{3}$$

One can see that the differential variable $(\delta\alpha - \delta\beta)$ provides the mutual angle of plummets filtered from the deformational tilts background. For generality, we also included in the angular deviation of the beam γ_{art} — intentional (artificial)

deviation, led by the operator for different purposes; for example, to keep the light spot in the center of the rear (end) mirror (this was typical case in the VSR-1, VSR-2 series).

The algorithm presented by Eqs. (1)–(3) comes down to the observation of the differential deviations of both mirrors to the beam. Formally the own beam deviations are falling out (compensated). In practice, of course, the accuracy and measure of such compensation depend on the noise background of stochastic angular beam tremors (beam jitter), which, in the case of the presence of "white noise" component, can be suppressed only through the procedure of accumulation of measurements. The latter depends on the lifetime of the useful signal. The routine experience of improving the signal-to-noise ratio by accumulation allows us to count on a factor from 10 to 100, i.e. achieving $\mathrm{NSD}_\alpha = 10^{-10}\,\mathrm{rad/Hz^{1/2}}$.

5. Search for Inner Core Oscillation Triplet

As was mentioned above, the technical condition of the Virgo setup during the VSR-1, VSR-2 series, did not allow to carry on precision angular measurements described in the previous section. Instead, the attempt to detect traces of the "core oscillations signal" was performed using the data of longitudinal deformation.

For this purpose, a special coherent filtering algorithm was developed[31] to detect the Smylie "translational inner core modes" signal. The five-month data series VSR-2 was processed, and an empirical estimate of timing changes in the variance of deformation noise was extracted. When using this empirical knowledge, the upper bound for the amplitude of inner core translational mode oscillations was derived.

5.1. *Translation mode of core oscillation*

According to the Smylie,[32] a more general type of oscillations of the inner core supposes small deviations from the axis of Earth's rotation. The physical description of this process is much more complicated (compared to the Slichter mode) because one should take into account the Coriolis as well as Lorentz forces, magnetic field and currents in the core. Such physics leads to the coupling of the vibration and rotational degrees of freedom. As a result, a mode splitting occurs and appears their combinative frequencies.

In particular, the Smylie theory predicts the presence of a translational triplet of inner core oscillations: the central axial component with a period of ∼3.76 h, the retrograde component ∼3.01 h, and the prograde component ∼4.01 h. As in the case of the Slichter mode, the prediction of amplitude is an incorrect problem depending on the magnitude of the earthquakes and their ability to contribute to the energy in the oscillations of translation triplets.

An experimental search for signals from the translation mode had been carried out early by a large international group of gravimetrists (led by B. Ducarme) with help of a global network of superconducting gravimeters during a three-years-long observations.[33]

The group reported about a registering of Smylie's triplet. The equivalent noise background averaged over several gravimeters was estimated by the average spectral density of gravity acceleration amplitude $\Delta g/g \sim (3 \times 10^{-12})1/\mathrm{Hz}^{1/2}$. It was problematic to notice any triplet signal directly from the gravimeter's record.

Authors of Ref. 33 claimed that the translation mode registration follows from some additional analysis through the coherent filtering procedure using of prior (theoretical) information concerning of spectral structure of mode oscillations.

The indicated above the level of sensitivity (resolution) for a Virgo interferometer at quasi-static frequencies means the ability to distinguish between absolute value of arm variations of $\sim 0.01\,\mu$m with a total tidal amplitude of $\sim 150\,\mu$m. Although the actual sensitivity of the instrument during the VSR-2 series was at least on factor 3 worse, we performed some analysis of the data of this series in an attempt to find traces of the translational mode signal, to elaborate a filtering technique.

5.2. *Search for triplet oscillation in the data of VSR-2*

The VSR-2 series lasted from 07.06.2009 to 11.16.2009. The total recording time is 162 days, the length of useful (used) pieces is 138 days. The number of continuous pieces exceeding 12 h - 121, exceeding 24 h - 91. A piece of maximum length (without interruption) - 3.65 days.

At the stage of preliminary preparation of raw records, the massive tidal deformations were removed from the data using calculated theoretical curves. After this, the description of the model of residual data and the task of filtering were formulated as follows.

There are fragmentary records $x(t)$ of Virgo interferometer, which are an additive mixture of a weak signal (deformations caused by oscillations of the inner core) and noise, i.e. $x(t) = s(t) + n(t)$. The signal model is given by the Smylie translational triplet hypothesis:

$$s(t) = \lambda \sum_{i=1}^{3} A_i \cos(\omega_i t + \varphi_i), \tag{4}$$

where $\lambda = 1.0$ is the formal detection parameter: $\lambda = 1$ in presence of signal, $\lambda = 0$ in absence of signal.

The triplet frequencies are considered as known ones; the amplitudes and phases are arbitrary. The noise is represented by a mixture of the slow flicker component n_f[34,35] and a white Gaussian additive background n_0. The spectral density of flicker noise is taken in the specific form $N_f(\omega) = D/\omega^2$,[36] where the characteristic factor D should be estimated from experimental data. (In the classification of flicker noises,[34,35] a type with a spectrum proportional to ω^{-2} is called as the "random walk", but its nature is different from the thermal Brownian noise.)

Parameter D reflects an intensity of flicker noise and according to the general theory[37] might be empirically estimated through a variance $\sigma_\Delta^2 t$ at output of differential link $\Delta n(t;\Delta t) = n(t) - n(t+\Delta t)$. Applying experimental data to couple arbitrary composed differential links $(\Delta t_1, \Delta t_2)$ one can calculate the D parameter through the formula.[37]

$$D = \frac{\sigma^2(\Delta t_2) - \sigma^2(\Delta t_1)}{\Delta t_2 - \Delta t_1}. \tag{5}$$

The piecewise nature of the records makes it necessary to calculate the constant D separately for each continuous segment, taking into account the individual values of D_k. In the analysis of VSR-2 data, this procedure was performed. The results are shown in Fig. 7. That are D_k histograms as a function of the number of segment (proportion to the time of record) for both arms of Virgo. Knowledge of empirical estimates of D_k concretizes the noise background.

Additionally, we introduced the following simplification, reasonable in the filtering of narrowband signals. We assumed that in the filtering band (around each triplet frequency) the spectral density of flicker noise is constant and equal to $N_f(\omega_0)$, where ω_0 is the center frequency of the band. Then, the problem of detecting a weak signal (Smylie triplet) in the framework of likelihood maximum algorithm is reduced to constructing a likelihood functional (at each interval of record) for a signal of a given shape against a white Gaussian noise with spectral density

$$N_k(\omega_0) = \frac{D_k}{\omega_0^2} + N_0, \tag{6}$$

where N_0 is the spectral density of additive background n_0. This formula is written for the individual k-th segment of data.

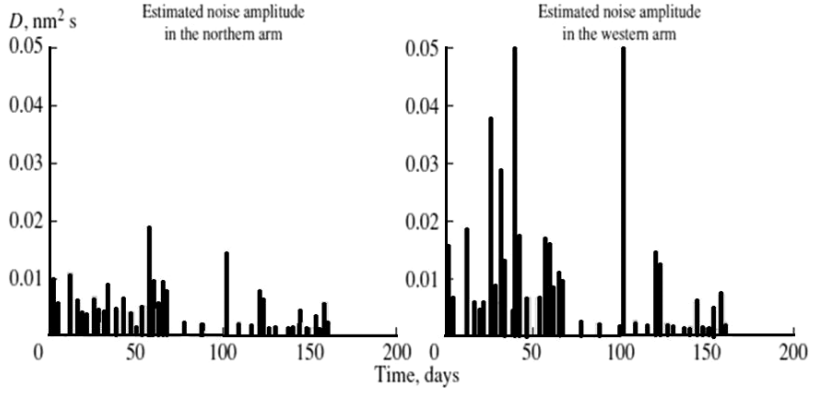

Fig. 7. Flicker noise parameter D_k histogram; VSR-2 data: (a) north arm, (b) west arm.

Assuming the independence of noises on individual intervals of record, one can compose the full functionality of likelihood ratio as the product

$$\Lambda[x(t)] = \prod_{k=1}^{m} \Lambda_k[x_k(t)]. \tag{7}$$

The task of maximizing of likelihood ratio functional on the Gaussian white noise in principle can be solved analytically. In Ref. 31, it was done numerically through the Monte Carlo simulation of $\Lambda(x(t))$ distribution with an estimation of detection threshold for Virgo data. No signal was registered.

Using the empirical data D_k of histograms (Fig. 7), we repeated this analysis in the frame of generalized likelihood ratio algorithm,[37] in which their likelihood estimates replaced the unknown parameters (phases φ_i and amplitudes A_i). The standard techniques[37] leads to the optimal observable variable $z_i = \ln\Lambda(x(t))$ (see Appendix). Under condition $\lambda = 1$ the optimal variable z_i is proportional to the ξ_i^2 — the sum of triplet matched filter outputs in square (see Appendix). After summarizing along with the large number of record pieces $m \geq 1$, it obeys the normal statistics (although at the individual piece of record it was the Rayleigh-Rician variable.[37])

Convention rule of the positive decision (i.e. $\lambda = 1$) corresponds to the situation when the optimal variable exceeds the threshold defined (in our case) by the probability integral or error function (see Appendix). The complete statistical error is coupled with the signal/noise ratio q by the following formula:

$$q = u_{1-\alpha} - u_{\beta} \tag{8}$$

where u_p is the quintile of the normal distribution $\Phi(u_p) = p$ (the α is the false alarm probability, the β in the false dismissal probability).

Our analysis of the data VSR-2 in the frame of the procedure described above results in the following conclusion. For more-less acceptable level of statistical errors ($\alpha = 0.1, \beta = 0.3$) the triplet detection threshold C_i could be overcome for relatively large signal/noise ratio $q \geq 30$. It corresponds to the strain level $\Delta L/L \approx 10^{-9}$ and gravity acceleration $\Delta g \approx 1\,\mu$Gal. This is the upper limit of core oscillation effect following from our measurements. It is equivalent to a noise 50 times above the cryogenic gravimeter noise.[33]

6. Discussion of Method and Results

It is useful to emphasize once again that the Virgo interferometer measures only differential deformation in two perpendicular directions. This instrument is optimally designed to detect tidal effects and it is in principle possible to detect the gradient of the ground gravitational field.

Perturbations of terrestrial areas (where seismically isolated suspensions are located) are the result of many influences, usually overlapped, which are difficult to resolved and distinguished. Suspension of test masses plays a decisive role here.

At a low-frequency, the test mass is no longer free in the plane normal to the suspension. The mechanical disturbances arising in this plane are compensated by a system using global and local feedback signals. Global correction signals are produced using the main beam, the spatial position of which is fixed (preserved) at frequencies where the system is well seismically isolated ($f > 10\,\text{Hz}$). Local correction signals are induced by a set of auxiliary optical position sensors (optical levers) for each mirror suspension.

The correct operation of the inverted IP pendulum has a decisive role on the quality of recording of deformations in the Virgo's arms. The first natural question is: to what extent do the IP correction signals reflect the real deformation of the underlying Earth's surface (when controlling the distance between the hanging mirrors)? The question is not trivial because the gravitational effect on the interferometer has two components. One of them is the direct influence of gravity acceleration vectors on test masses, and the other is the tidal deformation of the soil, which is also caused by gravity. Also, local non-gravitational disturbances may be imposed. Among them are thermal, mechanical drifts and environmental noises. To mitigate those effects, it is usual to implement specific environmental and technical measures.

(*A*) *Strain measurement over IP with LVDT*

(i) The mechanical drifts of SA suspensions, as well as thermoelastic variations, the influence of groundwater, and wind load on towers, induce spurious LVDT signals on the upper SA platform. On average, these signals are small and do not have a tidal periodicity. When processing the test observation series, they were not compensated. The gravitational effect of groundwater varies greatly seasonally, and after heavy rains, i.e. lies in the frequency range far from the characteristic core oscillation frequency $\sim 1/(4 \times 3600)\,\text{Hz}$. Tidal groundwater variations are part of the total tidal deformation of the local geographic area, contributing to the estimation of amplitude delta factor and phase delay.

(ii) Due to the active stabilization of temperature inside the towers — the so-called Super-Attenuator (SA) and payload undergo the isotropic expansion of the order of the several micrometers with a daily cycle. This expansion is negligible with respect to tidal deformation. The influence of temperature on the vertical degree of freedom is more effective because the range of variations is up to 100 μm (at the interval 24 h from day to night). However, the total length of the suspension chain is actively controlled, ensuring a holding accuracy of few microns.

(iii) The arm's length is fixed using the global control signal (the error signal comes from arm FP cavity). It is recalculated for the upper stage of SA. In this state, the LVDT is a top-level local monitoring sensor. At the test stand, LVDT accuracy is pretty good (RMS) < 0.05 microns (which corresponds to the displacement 0.01 microns in the 100 Hz band). However, for LVDT,

as an IP monitor on a separate SA, the accuracy is on half order of magnitude worse, i.e. (RMS) $\sim$ 0.1 micron. It is the result of the mixing of the IP control signal of position (LVDT) and acceleration (Accelerometers). The degree of contamination of the position correction signal in the frequency range $(10^{-5}-10^{-3})$ Hz depends on the instability of such weather conditions as wind, precipitation.

In total, for differential tidal deformations monitored by IP, the error in estimating the mutual movement of SA towers due to nongravitational mechanical noise background can be conservatively assessed about 10%.

(*B*) *Results of VRS*-1 *and VRS*-2 *observations*

In our discussion of the results of strain records in the VSR-1, VSR-2 series, it is useful to give the following comment:

Figure 2 compares the experimental curves with theoretical. These are theoretical curves calculated using the software ETGTAB (Wenzel)[19] for a given location (coordinates) and at the same time intervals as the acquired data. The phase of the signals did not change (as in the recording). The amplitude of the theoretical signal is calculated, taking into account the scaling factor of the feedback signals.

There is a noticeable difference in the magnitude of the spectral amplitudes in Fig. 3 for the northern and western arms. The matter is the following. According to the theory, the amplitudes of tidal waves in the East–West direction are always more significant than the amplitudes of tidal waves in the North–South direction. It is because the Earth's equatorial plane is always located near the plane of the ecliptic, where the influence of the tidal potential of the Sun and Moon is more effective than elsewhere.

Also, there is a difference between the spectral values of daily harmonics in Fig. 3 and of the amplitude delta factor estimation in the text. Our answer is the delta factors and phase shifts shown in Sec. 3 were obtained by the maximum likelihood method from the selected highest quality pieces of records VSR-1 and VSR-2 (Figs. 2(c) and 2(d)). On the contrary, the spectra were built using all available VSR-1 and VSR-2 data, in which there were such data as in Figs. 2(a) and 2(b). There were lots much worse than in these figures. One can notice that the data for P1 mode in 6 and 7 columns of Table 1 are missing. The reason is that the amplitudes of these harmonics are small and the recording time of VSR-2 was insufficient for their resolution in the tidal spectrum.

(*C*) *Angular gravity gradiometer*

Our proposal of using Virgo as a new instrument the angular gravity gradiometer encounters with the following questions:

(i) Could the use of IP be an obstacle to the realization of this idea? In our opinion IP does not basically distort the tilt of the mirror with respect to the beam,

moving the mirror parallel to itself. The angular error introduced by IP has the order of the fraction of its nongravitational noise i.e. no more than 10%.

(ii) It is not clear whether a realistic earthquake or other phenomena can excite oscillations of the inner core with amplitude on the order of $r = 1\,\mathrm{m}$. Here one could refer to the such argumentation. Under the ratio of the inner core mass to the Earth mass $m/M = 7.5 \cdot 10^{-4}$ and the oscillation period $\tau = 4\,\mathrm{h}$, the oscillation energy will be $E \leq 3 \cdot 10^{21}$ erg for the amplitude of 1 m. Geophysical estimates for short small energy variations during earthquakes and jumps in Earth's rotation reach $\sim 10^{22}$ erg.[2,8] Another argument for the admissibility of an amplitude of 1 m is a comparison of the oscillation power $P = \omega_o\, E \leq 10^{18}$ erg/s with a large total thermal flux emitted by the Earth $\sim 3 \cdot 10^{19}$ erg/s.[2,8]

(iii) The plummet deviation signal depends on the distance between the center of gravity of the mirror and of suspension point. In Virgo system a distance between the center of mirror and marionette is equal to 0.7 m. Does it mean that the angular sensitivity may not be too good compared to conventional tilt meters? In conventional tiltmeters, tilt monitoring is based on the movement of test mass surrounded by sensors (usually capacitive). The amount of movement depends linearly on the length of the suspension (for small deviations). In Virgo, using the alignment technique, monitoring is based on the principle of distinguishing spatial modes of FP cavity. There is no longer any dependence on the length of the suspension. It is important that the signal-to-noise ratio for the angular gradiometer can be high by eliminating the deformation component of the noise correlated in the angular signals of the shoulder FP cavities (Sec. 4).

7. Conclusions

After the discussion carried out above, we would like to formulate the main results of the research presented in this paper.

(1) The possibility of using the Virgo laser gravitational-wave interferometer as a geophysical instrument (two-coordinate tensometer) due to signals in the position control circuits of test mass mirrors proved experimentally.

(2) To our knowledge, the reconstruction of tidal deformation was performed for the first time using a 3-km-long interferometer with suspended mirrors and arms orientated along parallel and meridian directions in 2007–2009. The obtained spectra confirm the theory of tide (it was shown the possibility of properly reconstruction the relative amplitudes of main tidal harmonics S2, M2, S1, M1 registered in the arms of interferometer). Large absolute values of tidal displacements (150–200 μm) allows in principle the achievement of a high resolution in observation of the spectra details. The only condition is the capability of stable long-time operation of the instrument.

(3) For the Virgo interferometer, theoretical estimates were obtained for relation of signal-to-noise necessities for detection of weak gravitational perturbations induced by oscillations of the Earth's inner core. Based on the trend data of observational run VSR-2, the search for traces of the inner core translational mode was carried out. The upper limit of the amplitude of this effect was experimentally established.
(4) The possibility of using the Virgo installation as a new geophysical device (an angular gravity gradiometer) was proved at the principle level. It can measure pure gravitational perturbations through the mutual deflection of spatially separated plumb lines. From a physical point of view, this is a measurement of the spatial derivative of the gravity vector along the surface of the geoid. Thus, a new tool — an angular gravity gradiometer — is an addition to the geodetic instruments for deviating a plumb line. A scheme has been developed for compensating of the deformation component in the mutual angle of the front and end mirror's suspensions.

As a final remark, we would like to emphasize that the modern technical condition of the Virgo interferometer is essentially better adapted for the parallel geophysical measurements than it was in 2009–2010.

After the detection of a triple event of BBH by the LIGO — VIRGO network GW170814 and the reconstruction of the BNS coalescence GW170814, during the observational run LV-02,[38] LIGO and VIRGO detectors have been upgraded to detect more events with a larger rate of events. In this context, VIRGO joined the new observational run LV-O3 since 01.04.19, with a significantly high duty cycle figure 87%. Since this run (O3) is supposed to last for one year, a large amount of data, through control and error signals outside of the GW detection bandwidth, will be available soon for the investigation.

Acknowledgments

Authors thank EGO Directorate (European Gravitational Observatory in Cascina) and Virgo colleagues at the detector site, as P. Ruggi and I. Fiori, for their precious suggestions concerning the measurements done in the past as well as in the perspective of future geodynamical studies. We would also like to gratefully recall Adalberto Giazotto, with Alain Brillet founder of Virgo, who was a great enthusiast in detecting of the inner Earth's core oscillations with the Virgo interferometer.

This work was supported partly by the Russian national grant RFBR 19-29-11010.

Appendix A

Let's consider the stochastic process

$$x(t) = \lambda \sum_{i=1}^{3} \underbrace{A_i \cos(\omega_i t + \varphi_i)}_{s_i(t)} + n(t), \quad 0 \le t \le T, \tag{A.1}$$

where the $s(t)$ is the signal depending on unknown parameters $A_1,\ A_2,\ A_3,\ \varphi_1,\ \varphi_2,\ \varphi_3,\ \lambda = (0,1)$ — formal detection parameter, $n(t)$ — additive gaussian noise background. The process $s(t)$ is observed on separate time intervals $\{t_k, t_k + \Delta T_k\}$, $k = \overline{1,\ m}$, where ΔT_k is the duration of the k-interval i.e.

$$x(t) \to \Delta x(t) = \sum_{k=1}^{m} x_k(t). \tag{A.2}$$

Here, the notations are

$$x_k(t) = \lambda \sum_{k=1}^{3} \underbrace{A_i \cos(\omega_i t + \varphi_{ik})}_{s_{ik}(t)} + n_k(t), \quad t_k \le t \le (t_k + \Delta T_k). \tag{A.3}$$

$n_k(t)$ is the gaussian hindrance with the spectral dencity

$$N_k(\omega) = N_0 + \frac{D_k}{\omega^2}, \tag{A.4}$$

the substitution $\varphi_i \to \varphi_{ik}$ takes into account an uncertainty of time marks t_k.

In what follows, one supposes that (1) signals $s_{ik}(t)$ are orthogonal, (2) signal-to-noise ratio is small:

$$\frac{A_i^2 \Delta T_k}{2N_{ik}} \ll 1, \quad N_{ik} = N_k(\omega_i). \tag{A.5}$$

For simplification, let's suppose characteristics of detection (the false alarm error α_i and false dismission error β_i) are the same for all detection channels

$$\alpha_i = \alpha, \quad \beta_i = \beta. \quad i = 1, 2, 3. \tag{A.6}$$

The logarithm of likelyhood ration in the state $s(t) = s_i(t)$ is defined by the following expression:

$$z_i(x_k) = \frac{1}{2\kappa} \xi_i^2, \tag{A.7}$$

where

$$\kappa = \sum_{k=1}^{m} \frac{\Delta T_k}{2N_{ik}}; \quad \xi_i = \sum_{k=1}^{m} r_{ik}; \quad r_{ik} = \frac{1}{N_{ik}} \left(\int_{t_k}^{t_k + \Delta T_k} x_k(t)\ e^{j\omega_i t}\ dt \right). \tag{A.8}$$

Under the condition $m \gg 1$ according to the central limit theorem, ξ_i becomes asymptotically gaussian variable

$$M_1\{\xi_i \,|\, \lambda\} = \langle \xi_i \,|\, \lambda \rangle = \sum_{k=1}^{m} M_1\{r_{ik} \,|\, \lambda\}. \tag{A.9}$$

$$M_2\{\xi_i \,|\, \lambda\} = \langle \xi_i^2 \,|\, \lambda \rangle - \langle \xi_i \,|\, \lambda \rangle^2 = \sum_{k=1}^{m} M_2\{r_{ik} | \lambda\}. \tag{A.10}$$

Random values r_{ik} have the Releigh–Rice distribution[37] with parameters

$$\sigma_{ik}^2 = \frac{\Delta T_k}{2N_{ik}}; \quad \mu_{ik} = \frac{A_i \Delta T_k}{2N_{ik}}. \tag{A.11}$$

Solution "the signal $s_i(t)$ is detected" has to be accepted under the condition

$$\xi_i \geq C_{i\alpha}, \tag{A.12}$$

where $C_{i\alpha}$ is a threshold for the Neuman–Pirson detection strategy.[37]

Let's introduce the definition for the error function as

$$\Phi(x) = \frac{1}{\sqrt{2\pi}} \int_{-\infty}^{x} e^{-(t^2/2)} dt. \tag{A.13}$$

Then the errors of detection read as

$$\alpha = 1 - \Phi\left(\frac{C_{i\alpha} - M_1\{\xi_i \,|\, \lambda = 0\}}{\sqrt{M_2\{\xi_i|\lambda = 0\}}}\right), \tag{A.14}$$

$$\beta = \Phi\left(\frac{C_{i\alpha} - M_1\{\xi_i \,|\, \lambda = 1\}}{\sqrt{M_2\{\xi_i|\lambda = 0\}}}\right). \tag{A.15}$$

Finally, the general error of "right detection" can be presented by the formula

$$q = u_{1-\alpha} - u_\beta, \tag{A.16}$$

with the signal-to-noise ratio q

$$q = \frac{M_1\{\xi|\lambda = 1\} - M_1\{\xi|\lambda = 0\}}{\sqrt{M_2\{\xi_i|\lambda = 0\}}} \propto A_i^2, \tag{A.17}$$

where u_p is the quantile of the normal distribution $\Phi(u_p) = p$.

References

1. A. V. Kopaev and V. N. Rudenko, *JETP Lett.* **59**(9) (1994) 663.
2. V. N. Rudenko, *Phys. Lett. A.* **223** (1996) 421.
3. C. Bradaschia *et al.*, *Frontier Science Series* **32** (2000) 343.
4. S. L. Pasynok, V. N. Rudenko and A. V. Serdobolskii, *Meas. Tech.* **2** (2001) 3.
5. S. L. Pasynok, V. N. Rudenko and A. V. Serdobolskii, *Meas. Tech.* **3** (2001) 3.
6. V. V. Kulagin, S. L. Pasynok, V. N. Rudenko and A. V. Serdobolskii, *Proc. SPIE.* **4350** (2001) 178–189 (www.spie.org/).
7. V. N. Rudenko, A. V. Serdobolskii and K. Tsubono, *Class. Quantum Grav.* **20**(2) (2003) 317.
8. L. P. Grishchuk, V. V. Kulagin, V. N. Rudenko and A. V. Serdobolskii, *Class. Quantum Grav.* **22** (2005) 245.
9. KAGRA: 2.5 Generation Interferometric Gravitational Wave Detector, arXiv: 1811.08079v1 [gr-qc] 20 Nov 2018.
10. A. Araya *et al.*, *Earth, Planets Space* (2017) 69.
11. A. Giazotto, A. V. Gusev, S. Braccini, E. Majorana, M. Mantovani, P. Ruggi, V. N. Rudenko, A. A. Samoilenko, I. N. Tsybankov and V. D. Yushkin, Geo-applications of Virgo: basic principles and preliminary measurements. Virgo document publications (2009), http://www.ego-gw.it/VIR-003A-09.

12. R. W. P. Drever, J. L. Hall, F. W. Kowalski, J. Hough, G. M. Ford, A.J. Munley and H. Ward, *Appl. Phys. B* **31** (1983) 97.
13. E. Majorana, A. V. Gusev, A. A. Samoilenko, V. N. Rudenko, I. V. Tsybankov and V. D. Yushkin, Virgo geophysical channel: VSR-2/VSR-1 analysis. Virgo document publications (2010), http://www.ego-gw.it/VIR-0627A-10.
14. F. Acernese *et al.*, *Astropartiche Phys.* **33** (2010) 131.
15. A. Melissinos, Proc. MG-12 **part C** (World Scientific, 2012), pp. 1718–1720.
16. A. Melissinos, On the Possible Detection of Low Frequency Periodic Signals in Gravitational Wave Interferometers, arXiv:1410.0854v1 [astro-ph.IM] 2 Oct 2014.
17. V. A. Kostelecky, A. C. Melissinos and M. Mewes, *Phys. Lett. B* **761** (2016) 11.
18. A. V. Gusev, V. N. Rudenko and I. S. Yudin, Low frequency signals of large-scale GW-interferometers, arXiv:1310.3104v1 [gr-qc] 11 Oct 2013 / *JETP* **146** (2014) 779.
19. H. G. Wenzel, *Bull. D'Inf. Marees Terr.* **124** (1996) 9425.
20. Y. Tamura, *Bulletin d' Information Marees Terrestres* **99** (1987) 6813.
21. https://en.wikipedia.org/wiki/Least_mean_squares_filter.
22. A. V. Gusev, A. B. Manukin, V. N. Rudenko, A. A. Samoilenko, I. V. Tsybankov, V. D. Yushkin, A. Giazotto, S. Braccini, E. Majorana, M. Mantovani and P. Ruggi, *Meas. Tech.* **52** (2009) 111.
23. https:// workarea.ego-gw.it/ ego2/virgo/ data-analysis/ location-of-virgo/ location-of-virgo.
24. P. Melchior, *The Earth Tides* (Pergamon Press, Oxford, New York, 1966).
25. Avsyuk Yu. N. *Izvestya, Phys. Earth.* **37** (2001) 897.
26. N. Avsyuk Yu and I. I. Suvorova, *Izvestya, Phys. Earth.* **42** (2006) 598.
27. A. Gurashvilli, Yu. Gusev, A. Manukin and A. Nikolaev, *Phys. Earth.* **5** (1999) 14.
28. L. B. Slichter, *Proc. Natl. Acad. Sci.* (USA) **47** (1961) 186.
29. C. Hirt and G. J. Seeber, *J. Geodesy.* **82** (2008) 347.
30. C. Hirt, *J. Geodesy.* **84** (2010) 179.
31. A. V. Gusev, V. N. Rudenko, I. V. Tsybankov and V. D. Yushkin, *Gravit. Cosmol.* **17** (2011) 76.
32. D. E. Smylie, *Science* **255** (1992) 1678.
33. N. Cartier *et al.*, *Phys. Earth Planet. Int.* **117** (2000) 3.
34. S. M. Rytov, Y. A. Kravtsov and V. I. Tatarskii, *Principles of Statistical Radiophysics* (1989).
35. V. Barnett and T. Lewis, *Outliers in Statistical Data*, 3rd edn. (John Wiley & Sons, Chichester, 1994), ISBN 0-471-93094-6.
36. Beccaria *et al.*, *Class. Quantum Grav.* **15** (1998) 3339.
37. B. R. Levin, *Statistical Radiotechnics Theory* (Sov.Radio, 1998).
38. https://arxiv.org/abs/1811.12907.